JOURNAL OF GEOPHYSICAL RESEARCH, VOL. ???, XXXX, DOI:10.1002/,

A linear scale height Chapman model supported by GNSS occultation measurements

G. Olivares-Pulido,[1] M. Hernandez-Pajares,[1] A. Aragón-Àngel,[2]

A. Garcia-Rigo[1]

[1]UPC-IonSAT, Barcelona, Spain

[2]European Commission, Joint Research Centre (JRC), Institute for the Protection and Security of the Citizen, Italy.

Abstract. GNSS radio occultations allow the sounding of the Earth's atmosphere, in particular the ionosphere. The physical observables estimated with this technique permit to test theoretical models of the electron density such as, for example, the Chapman and the Vary-Chap models. The former is characterized by a constant scale height, whereas the latter considers a more general function of the scale height with respect to height.

We propose to investigate the feasibility of the Vary-Chap model where the scale height varies linearly with respect to height. In order to test this hypothesis, the scale height data provided by radio occultations from a receiver on board a low Earth orbit (LEO) satellite, obtained by iterating with a local Chapman model at every point of the vertical profile provided by the GNSS satellite occultation, are fitted to height data by means of a linear least squares fit (LLS).

Results, based on FORMOSAT-3/COSMIC GPS occultation data inverted by means of the Improved Abel transform inversion technique (which takes into account horizontal electron content gradients), show that the scale height presents a more clear linear trend above the F2 layer peak height, h_m, which is in good agreement with the expected linear temperature dependence. Moreover, the parameters of the linear fit obtained during four representative days for all four seasons, depend significantly on local time and latitude, strongly suggesting that this model can be especially suitable to build realistic models of the electron density directly derived from GNSS occultation data.

1. Introduction

Since the early 1990s, Global Navigation Satellite Systems (GNSS), e.g. Global Positioning System (GPS), have provided observational data to estimate the global vertical electron content (VTEC) of the ionosphere *Hernandez-Pajares et al.* 2009 [@]. Namely, GNSS radio occultation (RO) technique is a method for the study of the ionosphere *Yunck et al.* 2001 [@] that is based on precise carrier dual-frequency phase measurements (L-band) of a GPS receiver on board a Low Earth Orbit (LEO) satellite tracking a rising or setting GPS satellite behind the limb of the Earth *Schreiner et al.* 1999 [@].

Observational data provided by GNSS are used to obtain 2D and 3D VTEC models *Schaer* 1999 [@]; *Schmidt et al.* 2008 [@]; *Juan et al.* 1997 [@]. In spite of the lack of GNSS ground receivers over the oceans and in the southern hemisphere, a good interpolation strategy may yield complete and robust estimation of global VTEC maps (see *Orus et al.* 2005 [@]).

Another method for retrieving ionospheric electron density is the Abel transform inversion *Jakowski et al.* 2002 [@], although the spherical symmetry assumption on the electron density distribution (electron density depends only on the radial distance) yields significant error. Improved versions are the separability hypothesis *Hernandez-Pajares et al.* 2000 [@] and electron density with horizontal gradients *Yue et al.* 2010 [@]; *Kulikov et al.* 2011 [@].

Empirical models supported by data such as *Angling & Cannon* 2004 [@] do not present large gaps of data at global scale, but they rely on climatology for initialization when no fresh data are available.

Another alternative to retrieve electron densities is ionospheric modeling from first principles *Hajj et al.* 2004 [@]; *Khattatov et al.* 2006 [@]. For example, a Chapman model (CM) *Chapman* 1931 [@] for the electron density function normalized by the vertical total electron content, a.k.a. the shape function, was proposed in *Hernandez-Pajares et al.* 2011 [@] in order to obtain a 4D electron density field from first principles. It showed good consistency between the observed and predicted scale heights, and the theoretical and observed electron density profile. Nevertheless, there was a lack of local time dependency in the CM scale height H directly observed from the electron density. In CM, H is assumed to be constant and equal in top and bottom parts of the electron density profile. In order to overcome the lack of consistency showed in *Hernandez-Pajares et al.* 2011 [@], in this paper we aim to elucidate whether a linear relationship of the scale height, H, with respect to height, h, is a more realistic model similarly to the Vary-Chap model *Nsumei et al.* 2012 [@]. This linear model would take into account the change of the scale height through different layers in the atmosphere while, at the same time, retains the mathematical simplicity of the CM *Fox* 1994 [@].

This paper is organized as follows: the second section describes the method used to fit the data obtained from FORMOSAT-3/COSMIC (henceforth, COSMIC - *Lei et al.* 2007 [@]) GPS occultation data. In the third section, results are shown. In the fourth section, we propose a linear monotonous evolution of temperature T in the atmosphere with respect to height h that is compatible with the linear evolution of the scale height, H. Finally, the fifth section contains concluding remarks.

2. Method

The first step consists in inverting all the observations corresponding to GPS-LEO occultations, which are fast events where the dual-frequency GPS measurements are recorded by the onboard GPS receiver below the local horizon of the LEO satellite. The inversion is done by a technique relatively simple, but performing with high accuracy and vertical resolution: the improved Abel transform inversion (see for instance *Hernandez-Pajares et al.* 2000 [@] and *Aragon et al.* 2011 [@]). By means of the inversion, electron density profiles (EDPs) are retrieved from the original GPS-LEO radio occultation measurements. At this point, a local scale height value can be computed from each electron density value along a given electron density vertical profile, by considering the Chapman model *Nsumei et al.* 2012 [@], which is a simple mathematical model able to account for the formation of ionized layers, in particular, and it is able to describe the major observed variations of the layers of the ionosphere, represented in Eq. 1.

$$\begin{array}{c} N = N_m \mathrm{e}^{k\left(1-z-\mathrm{e}^{-z}\right)} \\ \text{where } \; z = \frac{h-h_m}{H} \end{array} \quad \begin{cases} \text{Alpha} - \text{Chapman}: \; k = 1/2 \\ \text{Beta} - \text{Chapman}: \quad k = 1 \end{cases} \tag{1}$$

where N is the electron density at height h, N_m represents the maximum electron density at height h_m and H stands for the scale height. On the other hand the Vertical Total Electron Content (VTEC), predicted by the CM follows Eq. 2:

$$VTEC = \int_{h=70km}^{LEO} N \cdot dh \simeq \frac{\mathrm{e}^k \Gamma(k)}{k^k} N_m H \, . \tag{2}$$

Since most of the electron content is below the plasmasphere, we have adopted $k = 1/2$, thus better representing the predominant EDP. In this context there are at least two simple Chapman-model-based ways of obtaining the classical constant scale height H:

1. $< H_{iter} >$ from (1), for each h, iteratively (h_m and N_m are taken from the inverted occultation profile) and averaged over a range from $100\,km$ to $200\,km$ above the maximum electronic density height;

2. and H_{VTEC} from (2), by taking the corresponding VTEC (from the profile or from a global VTEC model or map) and maximum value of electron density maximum N_m.

The remarkable compatibility of these two different Chapman scale height determinations H_{VTEC} vs. $< H_{iter} >$ (day 100, 2010 with more than 1000 FS3/COSMIC occultations) from inverted EDPs can be seen in Fig. 1.

We can also look at the height dependence of $< H_{iter} >$ (i.e. without averaging): Fig. 2 shows the values for the scale height iteratively computed from data corresponging to a single RO COSMIC event obtained in 2010, day 100. Although there is only one day plotted, it is representative of a quiet-condition scenario. Using a linear least squares (LLS) algorithm we fit the scale height H obtained iteratively from the occultation data with the height above and below h_m. We assume that, although, in general, the relationship is linear, the slopes above the top and below the bottom sides may be different, namely:

$$\begin{cases} H_t(h) = \dfrac{\partial H_t}{\partial h}(h - h_m) + H_{0,t},\ \forall h \geq h_m \\ \\ H_b(h) = \dfrac{\partial H_b}{\partial h}(h - h_m) + H_{0,b},\ \forall h < h_m \end{cases}, \tag{3}$$

where H_t (H_b) stands for the scale height at the top (bottom) side, i.e. above (below) h_m, and h is the height. If there were just one ionospheric layer, as Eq. 1 assumes, then the scale height values would be equivalent at h_m, i.e. $H_{0,t} = H_{0,b}$.

Fig. 2 shows an example of the fit for the bottom (blue) and the top (red) sides. Very often it is difficult to fit a straight line at the bottom side due to the great dispersion of data. That typically comes from the presence of layers with different chemical composition

below the maximum of electron density and perturbations of the electron density such as scintillation.

Fig. 2 is representative of the data set. More often than not, above the maximum, the data is further linearly correlated with height than below. Therefore, we focused the analysis on the upper ionospheric layer, i.e above h_m and below the transition height to the plasmasphere (see for instance *Gonzalez-Casado et al.* 2013 [@]),which is the ionospheric region where the single Chapman layer hypothesis is more realistic.

2.1. The algorithm

The algorithm used for the LLS fit is summarized as follows:

1. A first interval is chosen with all data above h_m.

2. Then the LLS correlation coefficient r between H and h data is computed and used as a goodness-of-fit test. If $r > \epsilon$ (with $0 < \epsilon < 1$ standing for a threshold value for the correlation coefficient) and the EDP contains more than N_0 data (i.e. the minimum number of iterated scale heights), then the LLS fit is accepted.

3. Otherwise, the closest datum and the most distant datum to h_m are removed from the interval. Then the algorithm goes back to the second step for a new LLS analysis.

The iteration above is performed for each EDP until $r > \epsilon$ and, simultaneously, the number of data available for the LLS fit is larger than N_0. Should the number of data available for the LLS fit be smaller than N_0 or $r < \epsilon$, then the EDP is dismissed.

3. Results

Henceforth the results presented are the output of computations performed with $\epsilon = 0.95$ and $N_0 = 25$. There were some results with no physical meaning such as, for example,

$H_0 < 0$, which were removed. Moreover, those results for which $H_0 > 200\,km$ were considered as outliers and removed too. With these conditions, it was possible to fit straight lines by LLS for 2582 EDPs out of 3254, i.e. 79.35% of EDPs; namely, 72.21%, 80.80%, 84.85% and 77.23% for northern hemisphere (NH) winter, spring, summer and fall, respectively.

Figs. 3 (2011, day 46, NH winter), 4 (2010, day 100, NH spring), 5 (2009, day 172, NH summer) and 6 (2010, day 328, NH fall) summarize the results obtained for the parameter estimates and their dependency with local time (LT) and latitude (θ). There were no magnetic storms during these days, therefore they are considered as representative of quiet-conditions scenarios.

In general, the scale height at the maximum of the peak, H_0, and the derivative of the scale height with respect to height, $\partial H/\partial h$, show significant dependency on LT and θ.

The latitudinal distribution in NH winter (Fig. 3 top-right) and fall (Fig. 6 top-right) of H_0, on one hand, and the NH spring (Fig. 4 top-right) and summer (Fig. 5 top-right) on the other hand, are very similar between them and quite symmetric, consistently with the seasons swap between the NH and south hemisphere (SH).

The scale height reaches the biggest values in NH winter (Fig. 3 top), which, in general, ranges from 35 to $50\,km$. In NH spring H_0 remains constrained between 30 and $40\,km$. The minimum is reached in NH summer (Fig. 5 top-left) when H_0 is usually smaller than $40\,km$ and even smaller than $30\,km$ at dawn.

Figs. 3 and 6 top-right, NH winter and fall, respectively, show that the biggest values for the scale height are around the equator, whereas during NH spring and summer (Figs. 4 and 5 top-right, respectively) the biggest values are located at the poles.

The derivative of the scale height is always positive (Figs. 3-6 bottom) and it shows a symmetric distribution around noon for NH summer and fall (Figs. 5-6 bottom-left). It is very similar along the local time in NH winter and spring (Figs. 3 and 4 bottom-left). In NH summer the derivative reaches its maximum: $\partial H/\partial h \sim 0.15$ (Fig. 5 bottom-left). Finally, Figs. 3, 4 and 6 bottom-right show that in NH winter, spring and fall, respectively, the derivative is symmetric around the equator where, in general, the smallest values are located.

4. A Theoretical Assesment

The results presented in the previous section are not compatible with an electron density model that assumes a constant scale height. Furthermore, these results stronly support a linear function of the scale height with height. This is in good agreement with theoretical models such as, for example, the Vary-Chap model, which is a family of functions that assumes the scale height changes with height *Rishbeth* 1969 [@].

Despite of the strong evidence of a linear scale height, it still remains to be elucidated the physical explanation for this model. One possible explanation could be provided by the definition of the scale height, i.e. $H = k_B T/mg$ (with k_B the Boltzmann constant, T the temperature, m the molecular mass and g the acceleration of a free-falling body in the gravity field). Indeed, a monotonous (and positive) linear evolution of temperature T with h would also yield a linear dependency of H with h:

$$T(h) = T_0 + ah\,, \tag{4}$$

with T_0 a reference temperature and $a \equiv \partial T/\partial h$ standing for the positive temperature gradient.

Nevertheless, this explanation just transfers to the temperature field the question regarding the linear relationship. One simple hypothesis for the linear temperature may be the unbalanced energy rate in the ionosphere. Indeed, if the energy source (e.g. solar EUV flux) imposes on any disipative process, the temperature may increase in the ionosphere. For example, in the top side of the ionosphere the electron density decreases as the altitude increases. On the other hand, the solar EUV flux increases with height (at daytime). Consequently, as height increases, the electrons (actually, photoelectrons) are less likely to scatter with ions and neutral atmospheric gas particles and, at the same time, they absorve further energy from EUV flux, thus increasing their cooling time. If such cooling time is larger than the EUV-flux absortion time, then this unbalanced energetic process entails an increase in the electron temperature. Further work would be necessary in order to assess the validity of such hypothesis.

In addition to the linear temperature, according to Newton's law, the gravitational field also depends on the height:

$$g(h) = \frac{GM_\oplus}{(R_\oplus + h)^2} \tag{5}$$

where T is the temperature at height h, G is Newton's gravitational constant, $R_\oplus$ and $M_\oplus$ the radius and mass of Earth, respectively.

By substituting T (Eq. 4) and $g(h)$ in H it yields

$$H = \frac{k_B}{GM_\oplus m}(T_0 + ah)(R_\oplus + h)^2 \,. \tag{6}$$

If $R_\oplus \gg h$, then $(R_\oplus + h)^2 \approx R_\oplus^2(1 + 2x)$, with $x \equiv h/R_\oplus$, then the next formula follows

$$H \approx \frac{k_B R_\oplus^2 T_0}{GM_\oplus m}\left[1 + \left(\frac{2}{R_\oplus} + \frac{a}{T_0}\right)h\right] \tag{7}$$

The equation above can be rewrite in terms of $h - h_m$, thus leading to the following theoretical expressions for H_0 and the gradient of the scale height:

$$\begin{cases} H_0 = \dfrac{k_B R_\oplus^2 T_0}{G M_\oplus m}\left[1 + \left(\dfrac{2}{R_\oplus} + \dfrac{a}{T_0}\right) h_m\right] \\ \partial H/\partial h = \dfrac{k_B R_\oplus^2 T_0}{G M_\oplus m}\left(\dfrac{2}{R_\oplus} + \dfrac{a}{T_0}\right) \end{cases}, \tag{8}$$

For example, if $a \approx 0.31\, K/km$, for a layer made of monoatomic oxygen mainly at temperature $T_0 \approx 1000\, K$, then $\partial H/\partial h \approx 0.033$ and $H_0 \approx 65\, km$. The result for the derivative is slighty smaller than those shown in Figs. 3-6 (bottom). As for the theoretical result for H_0, it is above of those shown in Figs. 3-6 (top). Nevertheless, both of them are of the same order of magnitude with the ranges of H_0 and $\partial H/\partial h$ shown in Figs. 3-6.

Also note that through Chapman model, i.e. Eq. 1, the scale height and temperature are correlated with the electron density, which is in good agreement with *Su et al.* 2015 [@] and references therein.

5. Conclusions

The scale height data provided by GPS radio occultations from a receiver on board a LEO satellite, obtained by iterating with a local Chapman model at every point of the vertical profile provided by the GNSS satellite occultation after applying the improved Abel transform, have been fitted to height by means of an LLS method.

The results obtained by LLS strongly suggests that the scale height H is linearly correlated with the height h in the top layer of the ionosphere.

In general, the scale height and its gradient depend on LT and latitude, thus facilitating the future development of simple but realistic 4D electron density models directly derived from GNSS occultation measurements. These results are in good agreement with

Vary-Chap models with linear scale height. Nevertheless, it still remains pending further analysis regarding the seasonal dependency.

A prospective physical explanation for the linear scale height would be the imbalance between the heating and cooling time of the plasma. Indeed, an overheating of the electron density would yield a dependency of temperature with height and, consequently, a dependency of the scale height with height too. Further work would be necessary to assess the validity of this physical hypothesis.

References

Angling, M.J. and Cannon, P.S., Assimilation of radio occultation measurements into background ionospheric models, R. Sci., Vol. 39, 2004.

Aragon, A., Liou, Y., Lee, C., Reinisch, B., Hernandez-Pajares, M., Juan, J., Sanz, J. (2011): Improvement of retrieved FORMOSAT-3/COSMIC electron densities validated by ionospheric sounder measurements at Jicamarca.Radio science.46 - RS5001,pp. 1 - 12.01/09/2011.

Chapman, S., The absorption and dissociative or ionizing effect of monochromatic radiation in an atmosphere on a rotating earth, Proceedings of the Physical Society Vol. 43, pp. 26-45, 1931.

Fox, M.W., A simple, convenient formalism for electron density profiles, Radio Science, Vol. 29, Num. 6, pp. 1473-1491, 1994.

González-Casado, Juan, J.M., Hernández-Pajares, M. and Sanz, J., Two-component model of topside ionosphere electron density profiles retrieved from Global Navigation Satellite Systems radio occultations, Journal of Geophysical Research: Space Physics,

Vol. 118, pp. 7348-7359, doi:10.1002/2013JA019099, 2013.

Hajj G.A., Wilson, B.D., Wang, C., Pi, X., Rosen, L.G., Data assimilation of ground GPS total electron content into a physics-based ionospheric model by use of the Kalman filter, R. Sci., Vol. 39, 2004.

Hernández-Pajares, M., Juan J.M., Sanz, J., Improving the Abel inversion by adding ground GPS data to LEO radio occultations in ionospheric sounding, Geophys. Res. Lett., Vol. 27, No. 16, pp. 2473-2476, 2000.

Hernández-Pajares, M., Juan, J.M., Sanz, J., Orus, R., Garcia-Rigo, A., Feltens, J., Komjathy, A., Schaer, S.C., Krankowski, A., The IGS VTEC maps: a reliable source of ionospheric information since 1998, Journal of Geodesy, v. 83, pp. 263275, DOI 10.1007/s00190-008-0266-1, 2009.

Hernández-Pajares, M., Juan, J.M., Sanz, J., Monte, E., Aragón-Àngel, A. and García-Rigo, A., Looking for efficient and accurate ways of computing the global ionospheric electron density distribution from huge amounts of GNSS observations, oral presentation at EGU General Assembly 2011, Vienna, Austria, 03-08 April, 2011.

Jakowski N., Wehrenpfennig A., Heise S., Reigber Ch., Lhr H., Grunwaldt L., Meehan T., GPS Radio Occultation Measurements of the Ionosphere from CHAMP: Early Results, Geophys. Res. Lett., Vol. 29, No. 10, 10.1029/2001GL014364, 2002.

Juan, J.M., Rius, A., Hernández-Pajares, M. and Sanz, J., A two-layer model of the ionosphere using Global Positioning System data, Geophysical Res. Letters, Vol. 24, No.4, pp. 393-396, 1997.

Khattatov B., Murphy, M., Gnedin, M., Sheffel, J., Adams, J., Cruickshank, B., Yudin, V.,Fuller-rowell, T., Retterer, J., Ionospheric nowcasting via assimilation of GPS mea-

surements of ionospheric electron content in a global physics-based time-dependent model, Quarterly of the Royal Meteorological Society, Vol. 131, No. 613, pp. 3543-3559, 2006.

Kulikov, I., Mannucci, A.J. , Pi, X., Raymond, C., Hajj, G.A., Advances in Space Research, Vol. 47, pp. 289-295, 2011.

Lei J., Syndergaard S., Burns A.G., Solomon S.C., Wang W., Zeng Z., Roble R.G., Wu Q., Kuo Y.H., Holt J.M., Zhang S.R., Hysell D.L., Rodrigues F.S., Lin C.H., Comparison of COSMIC ionospheric measurements with ground-based observations and model predictions: preliminary results. J Geophys Res v. 112:A07308, doi:10.1029/2006JA012240, 2007.

Nsumei, P.A., Reinisch, B., Huang, X., Bilitza, D., New Vary-Chap Profile Of The Topside Ionosphere Electron Density Distribution For Use With The IRI Model And The Giro Real Time Data, Radio Science, doi:10.1029/2012RS004989, 2012.

Orus, R., Hernandez-Pajares, M., Juan, J.M., Sanz, J., Improvement of global ionospheric VTEC maps by using Kriging interpolation technique, Journal of Atmospheric and Solar-Terrestrial Physics, Vol. 67, pp. 1598-1609, 2005.

Rishbeth, H. and O.K. Garriott, Introduction to ionospheric physics, Academic Press, New York, 1969.

Schaer, S., Mapping and Predicting the Earths Ionosphere Using the Global Positioning System, Ph. D. Dissertation, Astronomical Institute, University of Berne, Berne, Switzerland, 25 March 1999.

Schmidt, M., Bilitza, D., Shum, C.K. and Zeilhofer, C., Regional 4-D modeling of the ionospheric electron density, Advances in Space Research Vol. 42, No. 4, pp. 782-790,

2008.

Schreiner, S., Sokolovskiy, S.V., Rocken, C., Hunt, D.C., Analysis and validation of GPS/MET in the ionosphere, Radio Science, v. 34(4), pp. 949966, 1999.

Su, F., Wang, W., Burns, A.G., Yue, X. and Zhu, F., The correlation between electron temperature and density in the topside ionosphere during 2006 - 2009, Journal of Geophysical Research: Space Physics, doi: 10.1002/2015JA021303

Yue, X., Schreiner, W.S., Lei, J., Sokolovskiy, S. V., Rocken, C., Hunt, D.C. and Kuo, Y.H., Error analysis of Abel retrieved electron density profiles from radio occultation measurements, Ann. Geophys., Vol. 28, pp. 217-222, 2010.

Yunck, T.P., Liu, C.H., Ware, R. A history of GPS sounding, in: Lee, L.C., Rocken, C., Kursinski, R. (Eds.), Applications of Constellation Observing System for Meteorology, Ionosphere & Climate. springer, Berlin, pp. 120, 2001.

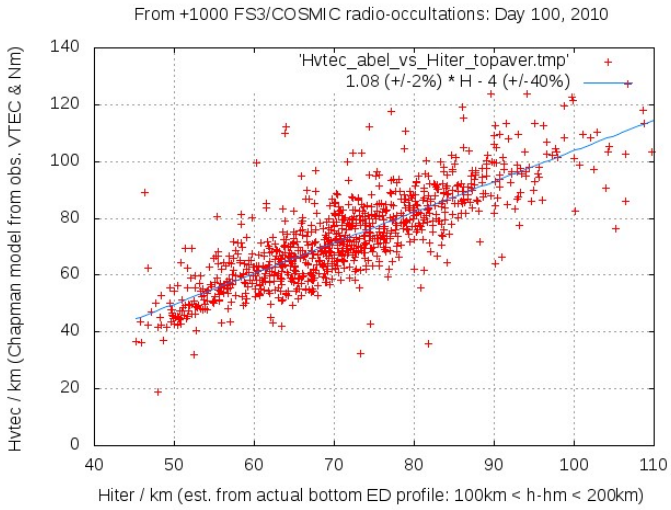

Figure 1. Comparison of Scale height determination from VTEC and maximum electron density versus a local iterative procedure, in +1000 electron density profiles derived from FORMOSAT3/COSMIC occultations (day 100 of 2010).

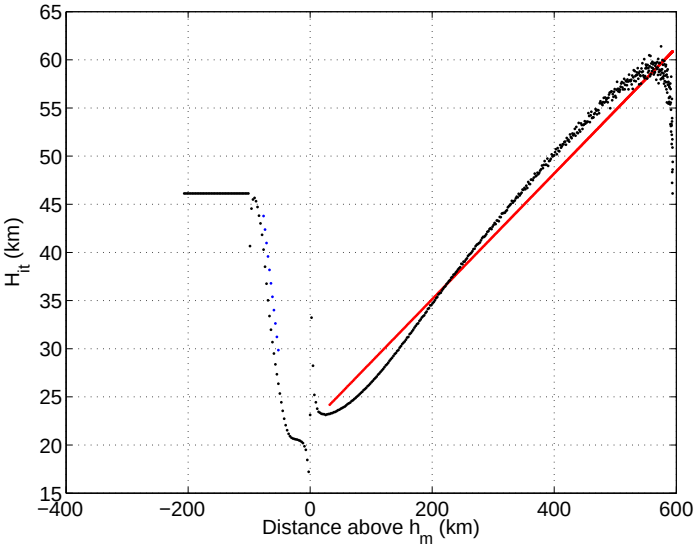

Figure 2. $< H_{iter} >$ vs. distance above the electronic density peak (h_m) during day 100 of 2010. Red/blue points correspond to the LLS fit above/below h_m. Black points correspond to occultation data gathered by COSMIC/FORMOSAT-3 receiver l211, observing GPS satellite PRN 7, starting at GPS time of 66842 seconds.

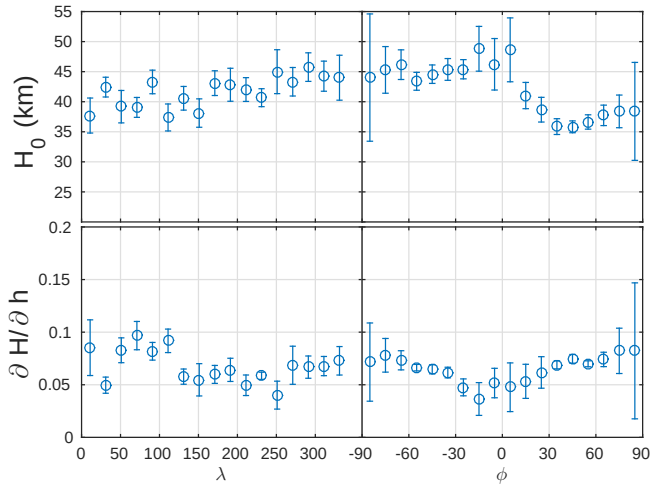

Figure 3. Scale height at maximum of electron density height vs. local time (top-left) and latitude (top-right), and derivative of scale height vs. local time (bottom-left) and latitude (bottom-right). Day 46, 2011, NH winter.

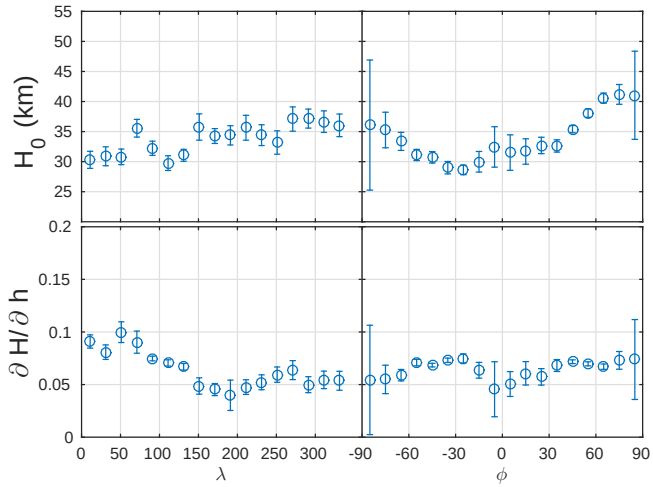

Figure 4. Scale height at maximum of electron density height vs. local time (top-left) and latitude (top-right), and derivative of scale height vs. local time (bottom-left) and latitude (bottom-right). Day 100, 2010, NH spring.

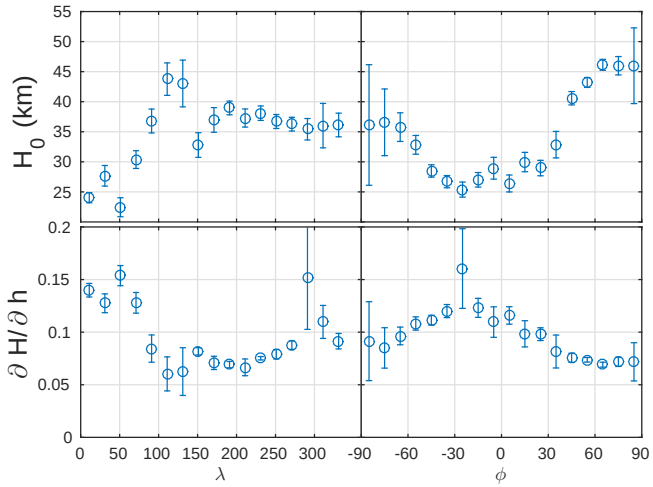

Figure 5. Scale height at maximum of electron density height vs. local time (top-left) and latitude (top-right), and derivative of scale height vs. local time (bottom-left) and latitude (bottom-right). Day 172, 2009, NH summer.

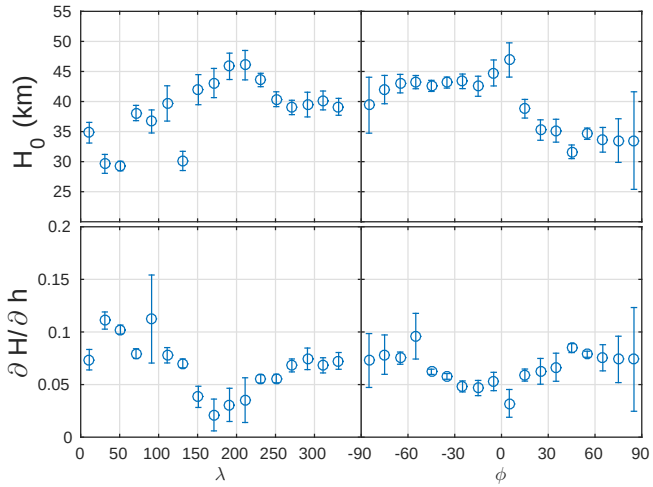

Figure 6. Scale height at maximum of electron density height vs. local time (top-left) and latitude (top-right), and derivative of scale height vs. local time (bottom-left) and latitude (bottom-right). Day 328, 2010, NH fall.